iScience

Article

A crosstalk between adhesion and phagocytosis integrates macrophage functions into their microenvironment

Graphical abstract

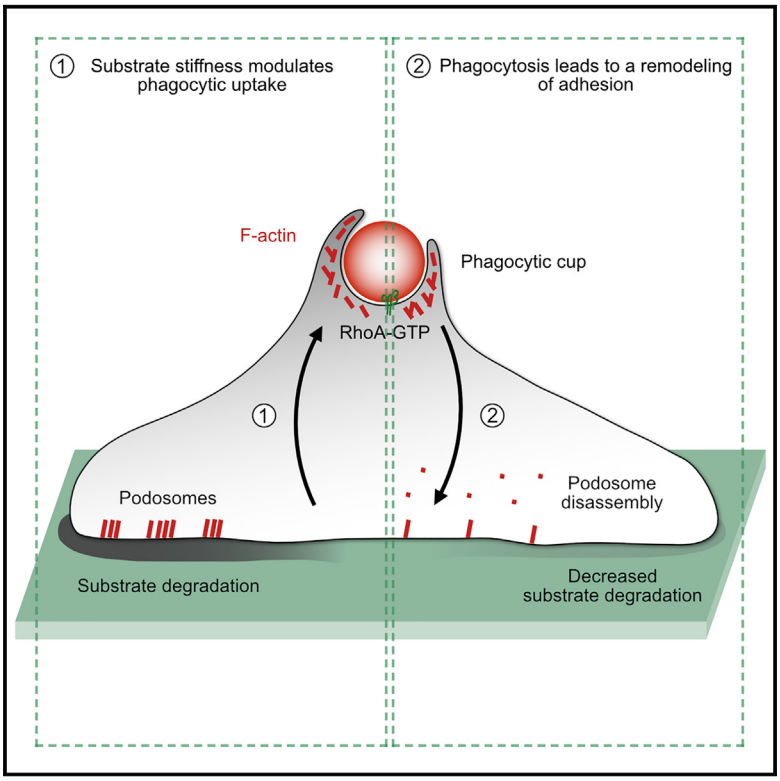

Highlights

- CR3-mediated phagocytosis by macrophages is modulated by substrate stiffness
- Phagocytosing macrophages interact more dynamically with their substrate
- Phagocytosis triggers transient podosome loss and decreased matrix degradation
- A crosstalk involving F-actin connects adhesion and phagocytosis in macrophages

Authors

Manon Depierre, Anna Mularski, Artur Ruppel, Christophe Le Clainche, Martial Balland, Florence Niedergang

Correspondence

florence.niedergang@inserm.fr

In brief

Cell biology; Organizational aspects of cell biology; Specialized functions of cells; Functional aspects of cell biology

Depierre et al., 2025, iScience *28*, 112067
April 18, 2025
https://doi.org/10.1016/j.isci.2025.112067

CellPress

iScience

CellPress
OPEN ACCESS

Article

A crosstalk between adhesion and phagocytosis integrates macrophage functions into their microenvironment

Manon Depierre,[1,5] Anna Mularski,[1,5] Artur Ruppel,[2,4] Christophe Le Clainche,[3] Martial Balland,[2] and Florence Niedergang[1,6,*]

[1]Université Paris Cité, Institut Cochin, INSERM, CNRS, 75014 Paris, France
[2]Université Grenoble Alpes, CNRS, Interdisciplinary Laboratory of Physics (LIPhy), Grenoble, France
[3]Université Paris-Saclay, CEA, CNRS, Institute for Integrative Biology of the Cell (I2BC), 91198 Gif-sur-Yvette, France
[4]Present address: Center de Recherche en Biologie cellulaire de Montpellier (CRBM), Université de Montpellier, CNRS, Montpellier, France
[5]These authors contributed equally
[6]Lead contact
*Correspondence: florence.niedergang@inserm.fr
https://doi.org/10.1016/j.isci.2025.112067

SUMMARY

Phagocytosis is the process of actin-dependent internalization and degradation of large particles. Macrophages, which are professional phagocytes, are present in all tissues and are, thus, exposed to environments with different mechanical properties. How mechanical cues from macrophages' environment affect their ability to phagocytose and, in turn, how phagocytosis influences how phagocytic cells interact with their environment remain poorly understood. We found that the ability of macrophages to perform phagocytosis varied with the substrate stiffness. Using live traction force microscopy, we showed that phagocytosing macrophages applied more dynamic traction forces to their substrate. In addition, integrin-mediated phagocytosis triggered a transient loss of podosomes that was associated with decreased degradation of the extracellular matrix, concomitantly with RhoA activation and F-actin recruitment at phagocytic cups. Overall, these results highlight a crosstalk between macrophage phagocytosis and cell adhesion. Mechanical properties of the microenvironment influence phagocytosis, which, in turn, impacts how macrophages interact with their surroundings.

INTRODUCTION

Phagocytosis is a mechanism of internalization and degradation of large particles (superior to 0.5 μm in diameter), such as microorganisms or cell debris. Target recognition is mediated by various phagocytic receptors, the best described of which are the Fcγ receptors (FcγR) and the integrin αMβ2, also known as the complement receptor 3 (CR3).[1,2] CR3 is a specific receptor for the opsonin iC3b, a protein fragment part of the complement system, but it was found to be able to bind to many other ligands.[3] Engagement of phagocytic receptors triggers signaling cascades resulting in the reorganization of the F-actin cytoskeleton, which drives particle engulfment.

In vertebrates, phagocytosis is a hallmark of specialized cells referred to as professional phagocytes, which include macrophages, dendritic cells, and neutrophils. This process is crucial for host defense against pathogens but also during development and for homeostasis as it allows tissue remodeling and disposal of dead cells.[4] Macrophages are present in virtually all tissues of the body. Tissue-resident macrophages not only share a common role as immune sentinels but also perform distinct functions depending on the organ.[5] These cells experience a broad range of mechanical cues as they can be exposed to environments with very different physical properties; as an example, organ rigidity (or stiffness, measured as the elastic modulus or Young's modulus) ranges from a few hundred Pa (lungs and brain) to a several dozen GPa (bone).[6] Even within an organ, tissue mechanics can be altered in disease conditions involving remodeling of the extracellular matrix (ECM),[7] such as fibrosis caused by chronic inflammation[8] and cancer progression.[6,9] The effect of mechanical cues (substrate stiffness and topography, hydrostatic pressure, and shear flow) on cell behavior has been extensively described, including for immune cells[10] and macrophages in particular.[11] Substrate rigidity is known to modulate macrophage inflammatory response, with macrophages seeded on stiff surfaces secreting higher amounts of pro-inflammatory cytokines in response to lipopolysaccharide (LPS) than those on soft surfaces.[12,13] Phagocytosis itself was found to be a mechanosensitive process as it is modulated by physical properties of the phagocytic targets.[14,15] However, how mechanical properties of the underlying substrate affect phagocytosis remains to be understood. Conversely, it is unclear how the process of phagocytosing can influence the way macrophages interact with their

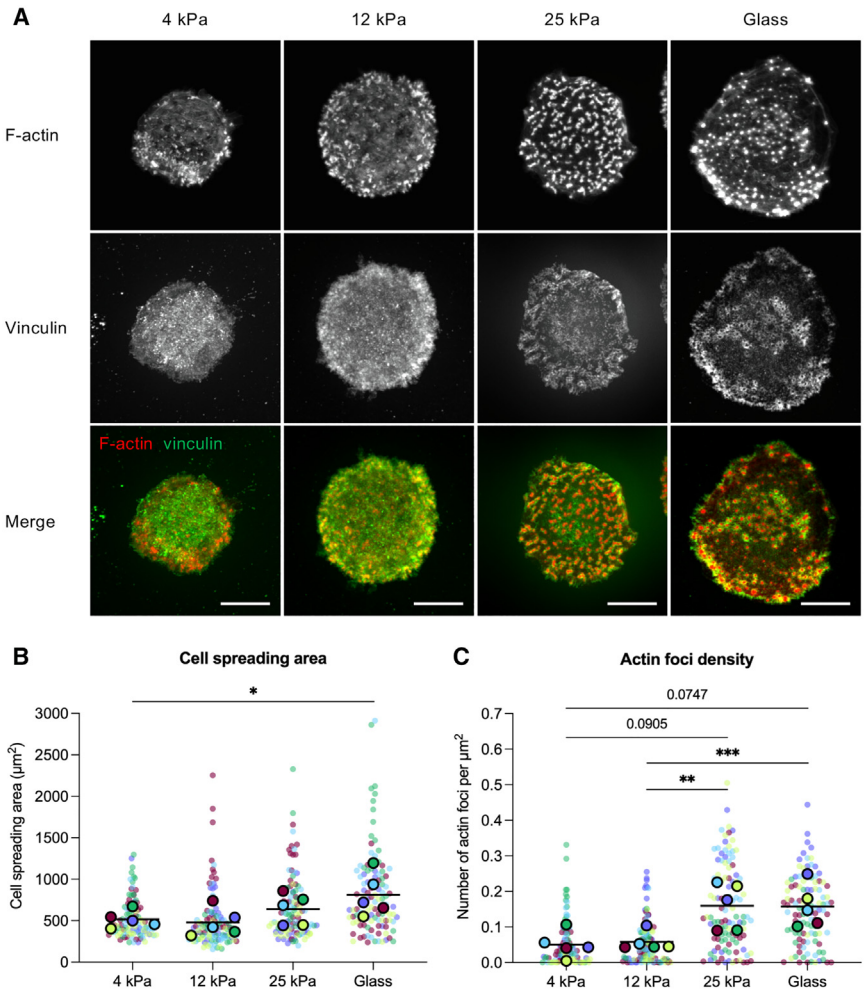

Figure 1. Primary human macrophage morphology and adhesion on substrates of different stiffnesses

hMDMs were seeded on fibronectin-coated polyacrylamide hydrogels or glass coverslips, incubated at 37°C for 4 h then fixed, permeabilized, and labeled with Alexa Fluor 488-conjugated phalloidin and a mouse antibody that recognizes vinculin followed by Alexa Fluor 647-labeled anti-mouse IgG antibodies.

(A) Representative confocal images (maximum z-projections) of macrophages seeded on 4 kPa, 12 kPa, or 25 kPa hydrogels or glass. Scale bar, 10 μm.

(B and C) Quantification of cell spreading area (B) and actin foci density (C) on the different substrates. Data from each donor is color coded: individual cells are represented as the smaller, lighter dots; means of all cells for each donor are shown as the bigger, darker dots with a black border. 10–30 cells were analyzed per condition and per donor. Horizontal bars represent the means of all donors. Ratio paired t tests were used to compare the means of all donors. *: p value < 0.05; **: p value < 0.01; ***: p value < 0.001.

environment and what its interplay with other cell functions might be. The existence of a crosstalk appears likely as phagocytosis employs a number of molecular actors that are also involved in cell adhesion, namely integrins and integrin-associated proteins, small GTPases of the Rho family, and F-actin.

Using primary human macrophages, we first showed that substrate stiffness modulates cell adhesion and CR3-mediated phagocytic uptake. Live traction force microscopy revealed that phagocytosing macrophages interact more dynamically with their substrate, and we found that phagocytosis leads to podosome disruption at the same time as F-actin recruitment at phagocytic cups, which was correlated to decreased degradation of the extracellular matrix.

RESULTS

Substrate stiffness affects macrophage adhesion structure formation but not cell spreading

Matrix rigidity is known to be a crucial factor in cell adhesion and spreading in many cell types, with consequences on cell behavior and fate.[16,17] Therefore, we first wanted to assess how substrate stiffness influenced these parameters in the case of primary human monocyte-derived macrophages (hMDMs). As previously described,[18] hMDMs constitutively form podosomes, a type of specialized cell-matrix adhesions that also participate in cell migration, degradation of the extracellular matrix, and mechanosensing of the cellular environment. They are characterized by a core of F-actin surrounded by a ring of adhesion plaque proteins (such as talin and vinculin) linked to the actin cytoskeleton. hMDMs were seeded on fibronectin-coated hydrogels of varying stiffnesses (from 4 to 25 kPa, a range of elastic moduli found in tissues) and allowed to re-adhere for 4 h. Glass coverslips, which are very stiff surfaces commonly used for cell biology studies, were also included as a familiar reference point. F-actin and vinculin at the ventral side of macrophages were observed by confocal microscopy (Figure 1A). Interestingly, cell spreading did not show major variations across the different hydrogels, only macrophages seeded on glass showed significantly increased spreading area compared to the other conditions (Figure 1B). However, quantification of F-actin-rich adhesion structures showed that their density increased with substrate stiffness, with a clear difference between macrophages seeded on 4 kPa and 12 kPa hydrogels on one hand, and macrophages on 25 kPa hydrogels and glass on the other hand (Figure 1C). Furthermore, vinculin was associated with the F-actin foci on 25 kPa hydrogels and glass, forming the rings characteristic of podosomes, but this was not the case on the softer substrates (Figure 1A). This indicates that substrate stiffness not only influences the number of adhesion structures formed by macrophages but also their architecture.

CR3-mediated phagocytic uptake varies with substrate stiffness

Phagocytosis is known to be a mechanosensitive process and many studies have focused on how the mechanical properties of the target influence its internalization. However, less is known about how other mechanical cues coming the cell's environment might impact phagocytosis. To address this question, we asked whether substrate rigidity could affect macrophage phagocytic capacity. hMDMs were seeded on fibronectin-coated hydrogels or on glass and, after 4 h, challenged with sheep red blood cells (RBCs) opsonized with IgM followed by complement (iC3b-IgM-RBCs). We assessed phagocytic uptake after 15 min by counting the number of internalized RBCs per cell (Figure 2A). The average numbers of internalized RBCs per cell from four independent experiments on different donors (Figure 2C) revealed differences in the macrophages' ability to phagocytose opsonized RBCs depending on the substrate stiffness. While phagocytic uptake was similar on 12 kPa and 25 kPa hydrogels, it was significantly lower than what was observed for cells on a very stiff surface (glass). Surprisingly, cells on 4 kPa hydrogels were able to internalize on average as many RBCs as their counterparts on glass, indicating that the relationship between substrate stiffness and phagocytic uptake might not be a linear one. Nonetheless, these results indicate that phagocytosis mediated by CR3 is sensitive to substrate rigidity and, thus, to the mechanical properties of the cell's environment. We next wondered if these differences in internalization stemmed from differences in RBC initial binding to macrophages at the start of the assay; in other words, if macrophages that phagocytosed a greater number of RBCs did so because they were able to capture a greater number of targets. Despite not being significant, the average numbers of associated (bound + internalized) RBCs per cell at 0 min (Figure 2B) showed a similar sensitivity to substrate stiffness than phagocytic uptake. This suggests that the differences in internalization might stem from differences in RBC association with macrophages at the start of the assay.

CR3 binding to its ligand on opsonized targets depends on its conformation. Like all integrins, CR3 can be found in a ''bent-closed'' conformation with a low affinity for its ligand or in an ''extended-open'' conformation with a high affinity for its ligand. Integrin conformational activation is known to be regulated by multiple external signals, including the extracellular matrix. We hypothesized that differences in CR3 conformational state depending on substrate stiffness might explain the differences in RBC association and, subsequently, internalization. To test this, we treated macrophages with phorbol 12-myristate 13-acetate (PMA) for 15 min prior to adding RBCs. PMA activates the protein kinase C (PKC), which leads to the inside-out activation of CR3. After PMA treatment, differences in RBC association across the different substrates at 0 min were no longer significant (Figure 2B), suggesting that these differences can indeed be explained by different CR3 conformational states. Interestingly, however, differences in phagocytic uptake remained even after PMA treatment, although to a lesser extent (Figure 2C). This indicates that the CR3 activation state does not explain fully the differences in phagocytic uptake depending on the substrate stiffness. When we calculated the phagocytosis efficiency, i.e., the percentage of bound RBCs that were internalized after 15 min, the differences between substrates were similar to those observed for phagocytic uptake (Figure 2D), suggesting a sensitivity to substrate stiffness in the internalization process by phagocytosis.

F-actin recruitment during phagocytosis varies with substrate stiffness

To better understand how substrate rigidity affects phagocytosis, we compared F-actin accumulation at the onset of phagocytosis on the different surfaces. hMDMs were fixed after 2 min of contact with opsonized RBCs and analyzed by confocal microscopy (Figure 2E). Quantification of the average numbers of actin cups around RBCs per cell (Figure 2F) showed differences across the different substrates that followed what was observed for phagocytic uptake after 15 min (Figure 2C). Macrophages on 12 kPa and 25 kPa hydrogels formed very few actin cups around RBCs after 2 min, while the number of actin cups was significantly higher on 4 kPa hydrogels and on a very stiff surface (glass). These results indicate that substrate stiffness affects F-actin recruitment around targets during phagocytosis, which could explain the subsequent differences in phagocytic uptake.

The traction forces of phagocytosing macrophages have a more isotropic arrangement than control cells

We asked if phagocytosis could affect the way macrophages interact with their substrate. For this, we developed a dedicated experimental set-up based on live traction force microscopy to monitor traction forces exerted by macrophages on their substrate during phagocytosis. hMDMs were allowed to adhere to fibronectin-coated 10 kPa polyacrylamide gels containing fluorescent beads and imaged live during phagocytosis of iC3b-IgM-RBCs. Traction stress was calculated from measured bead displacements, which were obtained by particle image velocimetry and single particle tracking (Figures 3A and 3B, Videos S1 and S2). We noticed a difference in the distribution of traction forces between control and phagocytosing macrophages: the traction forces of phagocytosing cells tended toward an isotropic arrangement more than those of control cells. To quantify the arrangement of cellular traction forces, we calculated the polar degree of control and phagocytosing cells. The polar degree indicates the degree of polarization of the force pattern: a cell with traction stress that corresponds to a polar degree of 0 has an isotropic arrangement of forces, while a cell with traction stress that corresponds to polar degree of 1 has a uniaxial arrangement. Interestingly, phagocytosing macrophages showed a significantly lower polar degree than control cells (Figures 3C and 3D), at both 0 (start of the assay) and 30 min.

Phagocytosing macrophages "knead" the substrate to a greater extent than control cells

In addition to a difference in the arrangement of traction forces between control and phagocytosing cells, we found a difference in the extent to which the traction stress of control and phagocytosing macrophages was observed to shift on the substrate. This characteristic of cells, which can also be described as ''kneading'' the surface, becomes apparent when tracking the change in position of the main tractions of the cells (Figures 4A–4C, Videos S3 and S4), and we observed the main traction of

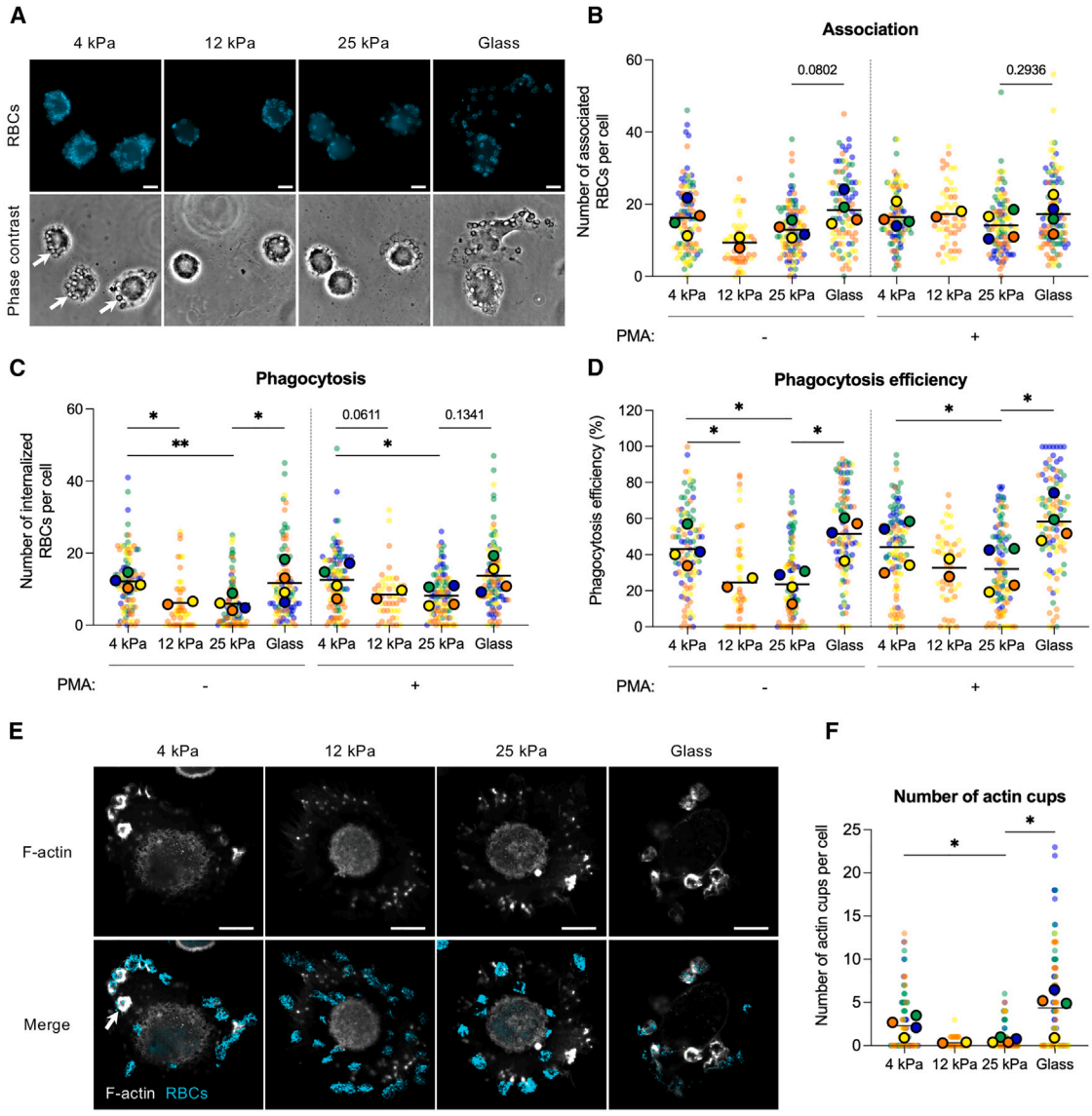

Figure 2. Integrin-mediated phagocytic uptake is modulated by substrate stiffness

hMDMs were seeded on fibronectin-coated polyacrylamide hydrogels or glass coverslips and incubated at 37°C for 4 h. Cells were pre-treated or not with 150 ng/mL PMA for 15 min, challenged with opsonized RBCs (iC3b-IgM-RBCs) and fixed immediately (time "0" min) or after 15 min at 37°C. Cells were then labeled with Alexa Fluor 488-conjugated phalloidin and a Cy3-labeled anti-rabbit antibodies that recognize the anti-sheep RBCs IgMs used to opsonize RBCs.

(A) Representative wide-field images of macrophages seeded on 4 kPa, 12 kPa, or 25 kPa hydrogels or glass and incubated with iC3b-IgM-RBCs for 15 min. Opsonized RBCs are shown in cyan in the upper panel and phase contrast images are shown in the lower panel, where phagosomes are visible (examples of phagosomes are shown by the white arrows). Scale bar, 10 μm.

(B and C) Quantification of RBC association at 0 min (B) and phagocytosis after 15 min (C) on the different substrates, with or without PMA pre-treatment. Association refers to both bound and internalized RBCs while phagocytosis only considers internalized RBCs.

(D) Phagocytosis efficiency after 15 min on the different substrates, with or without PMA pre-treatment, calculated as the percentage of bound RBCs that are internalized.

(E) Representative confocal images of macrophages seeded on 4 kPa, 12 kPa, or 25 kPa hydrogels or glass and incubated with iC3b-IgM-RBCs for 2 min. F-actin is shown in gray while RBCs are shown in cyan (white arrow shows one example of an actin cup). Scale bar, 10 μm.

(F) Quantification of the number of actin cups formed by macrophages after 2 min.

(B–D and F) Data from each donor is color coded: individual cells are represented as the smaller, lighter dots; means of all cells for each donor are shown as the bigger, darker dots with a black border. 25–30 cells were analyzed per condition and per donor. Horizontal bars represent the means of all donors. Ratio paired t tests were used to compare the means of all donors. *: p value < 0.05; **: p value < 0.01.

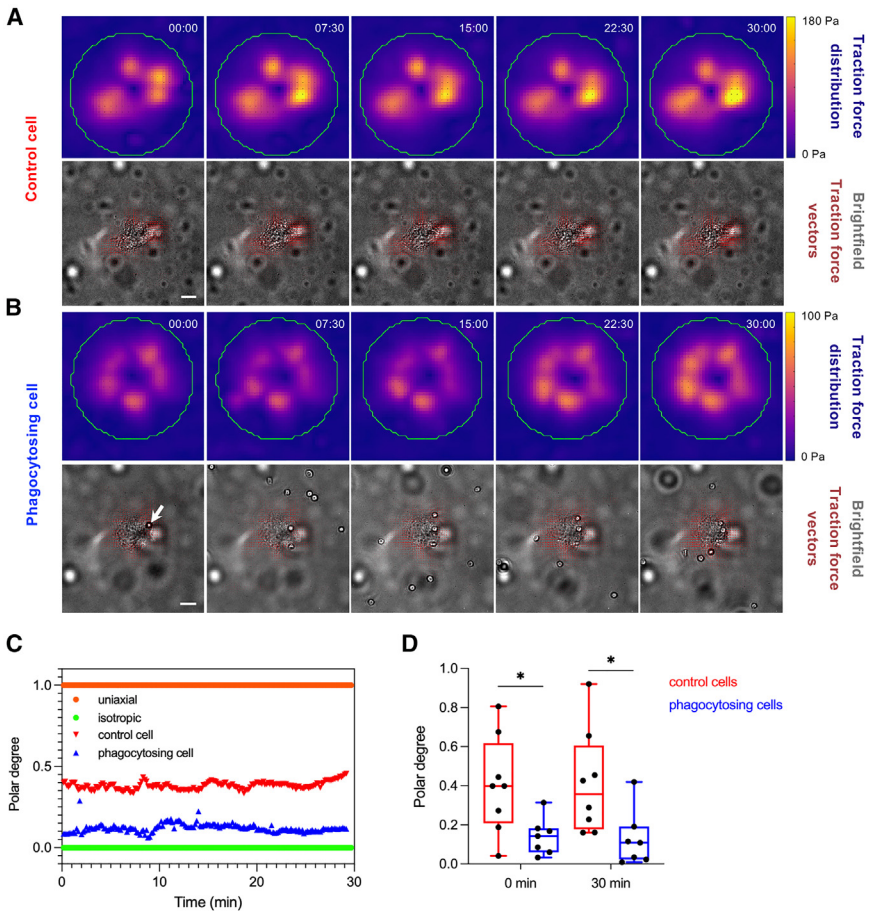

Figure 3. Analysis of the arrangement of traction forces exerted by cells on their substrate highlights differences between control and phagocytosing macrophages

hMDMs were seeded on fibronectin-coated 10 kPa polyacrylamide gels and incubated at 37°C for 4 h. Cells were challenged or not with opsonized RBCs (iC3b-IgM-RBCs) and imaged live for 30 min at 37°C.

(A and B) (Upper panel) Traction force distribution of a control cell (A) and a phagocytosing cell (B) at different time points; also see Videos S1 and S2. (Lower panel) Corresponding brightfield images with traction force vectors superimposed in red for the control cell (A) and the phagocytosing cell (B). Green circles represent the approximate outlines of the cells. One example of an RBC about to be internalized is depicted by the white arrow. Time is shown as minutes:seconds. Scale bar, 10 μm.

(C) Polar degree of the control cell (red) and the phagocytosing cell (blue) over the 30 min observation period. The orange line (polar degree equal to 1) corresponds to a theoretical situation with a purely uniaxial arrangement of traction forces and the green line (polar degree equal to 0) represents a purely isotropic arrangement.

(D) Polar degree of 8 control cells (red) and 7 phagocytosing cells (blue) from independent donors at 0 and 30 min. Unpaired t tests were used to compare the populations of control and phagocytosing cells at each time point. *: p value < 0.05.

phagocytosing cells shifted more on the surface. To quantify this, changes in main tractions (in deg) for control and phagocytosing cells were tracked during the observation period (Figure 4D). When comparing the standard deviations of the change in main traction for each cell in the two populations (Figure 4E), we found a significant increase in phagocytosing macrophages. There was no trend observable in the change in main traction that could be linked to the attachment of individual phagocytic targets or individual phagocytic events throughout the observation period. Therefore, phagocytosing cells knead the surface and interact more dynamically with it than control cells.

CR3-mediated phagocytosis leads to a loss of podosomes at the ventral side of macrophages

To better characterize the interactions of phagocytosing macrophages with their environment, we investigated if phagocytosis led to a modification of podosomes at the ventral side of macrophages. hMDMs seeded on glass coverslips were allowed to phagocytose iC3b-IgM-RBCs, fixed at different time points and analyzed by confocal microscopy. Podosome density was determined based on the F-actin staining. Because podosome density at steady state varied depending on the donor, results were expressed as fold change from the mean of the basal condition for each donor. We found that phagocytosis led a rapid decrease of macrophage podosome density, with a majority of cells having no or very few podosomes left after 2 min of contact with the RBCs (Figures 5A and 5B). This decrease seemed to be transient as we started to observe a recovery of podosome density after 15 min. Cell spreading area did not change over the time points studied (Figure 5C). Interestingly, podosome disruption coincided with the timing of F-actin recruitment at the phagocytic cup (at the dorsal side of macrophages). Macrophages with visible F-actin recruitment around RBCs displayed significantly decreased numbers of podosomes compared to macrophages with bound RBCs but no F-actin recruitment around targets (Figures 5D and 5E). This observation suggests the existence of a crosstalk involving the actin cytoskeleton between adhesion and phagocytic uptake in macrophages.

As podosome architecture is complex, we looked at the localization during phagocytosis of other proteins known to take part in podosome structure. At steady state, vinculin formed the characteristic ring around the F-actin foci at the ventral side of macrophages (Figure 6A, left). This organization was similarly disrupted during phagocytosis and vinculin was recruited to the phagocytic cup concomitantly with F-actin (Figure 6A, right). A similar pattern was observed for p34-Arc/ARPC2, a subunit of the human Arp2/3 protein complex (Figure 6B). Of note, active RhoA (RhoA-GTP), a small GTPase known to be a hallmark of CR3-mediated phagocytosis,[19,20] was not associated with podosomes at steady state but was found with F-actin around RBCs during phagocytosis (Figure 6C). This observation

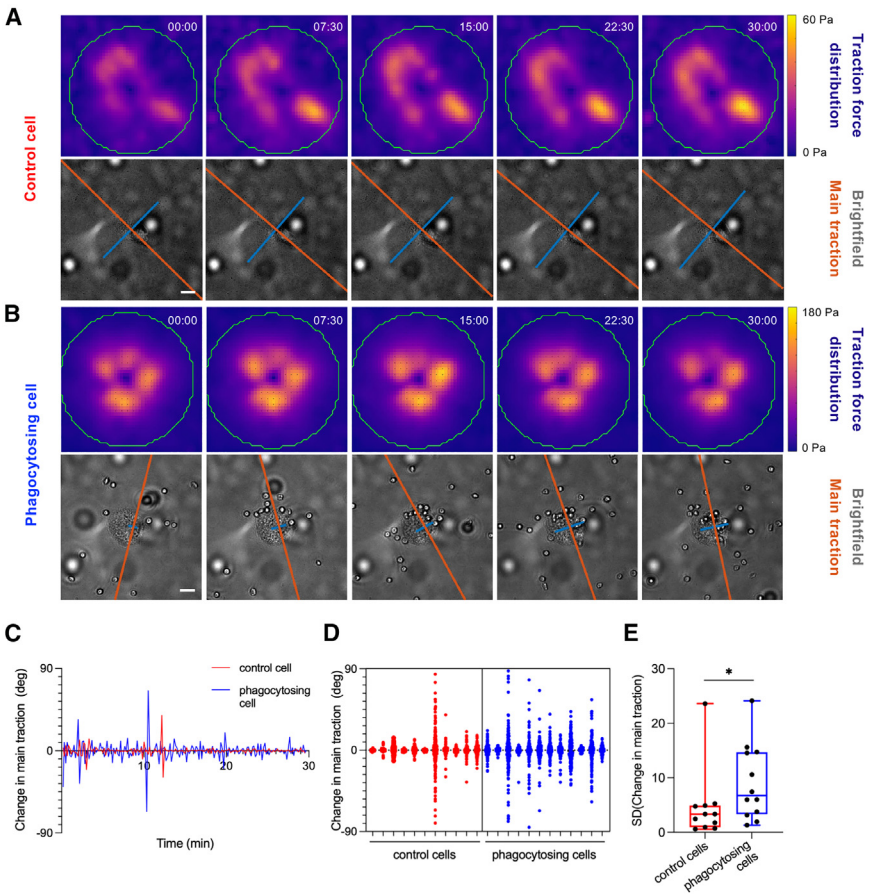

Figure 4. Phagocytosing macrophages show greater changes in their main traction than control cells

hMDMs were seeded on fibronectin-coated 10 kPa polyacrylamide gels and incubated at 37°C for 4 h. Cells were challenged or not with opsonized RBCs (iC3b-IgM-RBCs) and imaged live for 30 min at 37°C.

(A and B) (Upper panel) Traction force distribution of a control cell (A) and a phagocytosing cell (B) at different time points; also see Videos S3 and S4. (Lower panel) Corresponding brightfield images with main traction superimposed in orange for the control cell (A) and the phagocytosing cell (B). Green circles represent the approximate outlines of the cells. Time is shown as minutes:seconds. Scale bar, 10 μm.

(C) Change in main traction (in degrees) for the control cell (red) and the phagocytosing cell (blue) over the 30 min observation period.

(D) Change in main traction (in degrees) for 11 control cells (red) and 13 phagocytosing cells (blue) from independent donors observed for 30 min. Each column corresponds to a cell and each dot represents one change in main traction.

(E) Standard deviation of change in main traction for 11 control cells (red) and 13 phagocytosing cells (blue) over the 30 min observation period. A Mann-Whitney test was used to compare the populations of control and phagocytosing cells. *: p value < 0.05.

suggests that RhoA-mediated signaling drives the reorganization of the actin cytoskeleton.

Loss of podosomes during CR3-mediated phagocytosis is associated with decreased gelatin degradation

An important function of podosomes is the local degradation of the extracellular matrix, thanks to the recruitment of lytic enzymes.[21] Since phagocytosis led to the disruption of podosomes in macrophages, we wondered whether it also affected their ability to degrade components of the extracellular matrix. hMDMs were seeded on coverslips coated with fluorescent gelatin, challenged or not with iC3b-IgM-RBCs and gelatin degradation was assessed after 2 h (Figure 7A). The mean degradation area per cell was almost halved when macrophages were allowed to phagocytose RBCs (Figure 7B), indicating that their ability to degrade gelatin was decreased by phagocytosis.

Taken together, our results highlight the existence of a cross-talk involving the actin cytoskeleton in macrophages during CR3-mediated phagocytosis, with a connection between what happens at the dorsal side of the cells (phagocytosis) and at their ventral side (adhesion to the substrate). Macrophage adhesion is influenced by substrate stiffness, which also affects phagocytic uptake. Furthermore, macrophage adhesion is actively remodeled during phagocytosis, with functional consequences on degradation of the extracellular matrix.

DISCUSSION

In this study, we showed that phagocytosis, on the one hand, and cell adhesion and matrix degradation, on the other hand, are cell functions that inform one another in primary human macrophages.

Several aspects of macrophage behavior were previously shown to be influenced by substrate stiffness.[12,22,23] Using polyacrylamide gels of increasing elastic modulus, we observed differences in the formation and architecture of the F-actin-rich adhesion structures known as podosomes, which were promoted by substrate stiffness. This result is consistent with a previous study[24] that also demonstrated that podosomes have a mechanosensing activity that likely contributes to macrophages' probing of their microenvironment.[25]

When we subsequently evaluated phagocytosis mediated by CR3, we found that substrate stiffness modulated F-actin recruitment around targets and phagocytic uptake. Macrophages were on average able to phagocytose as many targets on the softer substrate tested (4 kPa) than on glass coverslips, while the number of internalized RBCs was significantly lower on the intermediate-to-high stiffness substrates (12 and 25 kPa); F-actin accumulation at phagocytic cups followed a similar trend. Our results suggest that, over the physiological range of hydrogel stiffnesses tested, phagocytic uptake is

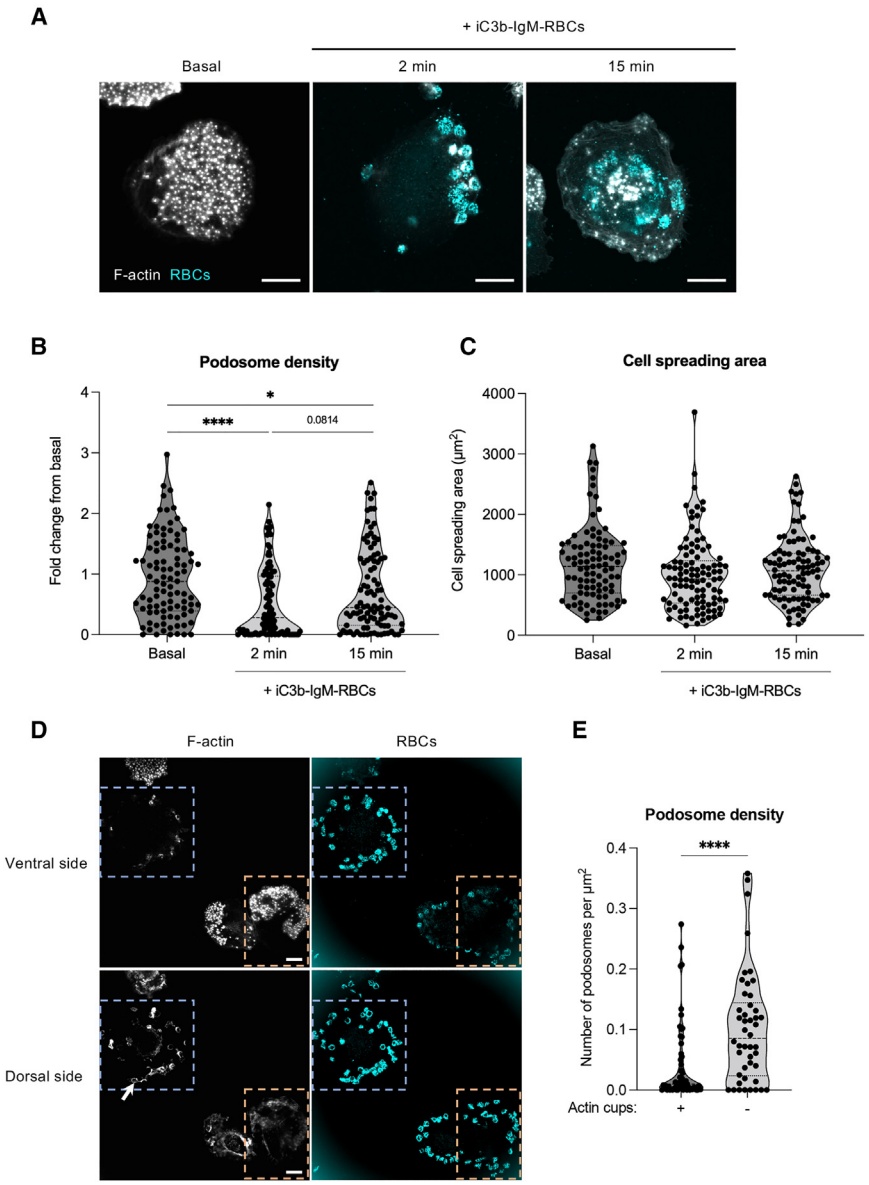

Figure 5. Phagocytosis is associated with the disruption of podosomes at the ventral side of macrophages

hMDMs were seeded on glass coverslips, incubated at 37°C for 4 h and challenged with opsonized RBCs (iC3b-IgM-RBCs). Cells were fixed at steady state (basal) or after a 2- or 15-min incubation with RBCs, permeabilized and labeled with Alexa Fluor 488-conjugated phalloidin and Cy3-labeled anti-rabbit antibodies that recognize the anti-sheep RBCs IgMs used to opsonize RBCs.

(A) Representative confocal images of the ventral side of macrophages (close to the coverslip) at steady state (basal) or after 2 or 15 min with RBCs. F-actin is shown in gray while RBCs are shown in cyan. Scale bar, 10 μm.

(B and C) Quantification of podosome density (B) and cell spreading area (C) at the different time points. Each dot represents an individual cell; data are pooled from 3 independent donors with 25–30 cells per condition and per donor. Because podosome density at steady state across the different donors is heterogenous, results are expressed as fold change from the mean of all cells in the basal condition for each donor. A Kruskal-Wallis test was used for comparison of multiple groups in (B).

(D) Representative confocal images of the ventral side (upper panel) or dorsal side (lower panel) of macrophages after 2 min with RBCs. F-actin is shown in gray while RBCs are shown in cyan. Blue dashed box highlights a macrophage with F-actin recruitment around multiple RBCs on the dorsal side (white arrow shows one example of an actin cup) and no podosome on the ventral side; orange dashed box shows a macrophage with no F-actin recruitment around bound RBCs on the dorsal side and many podosomes on the ventral side. Scale bar, 10 μm.

(E) Quantification of podosome density after 2 min with RBCs, comparing macrophages with F-actin recruitment around RBCs (actin cups) or not. Each dot represents an individual cell; data are pooled from 3 independent donors with 25–30 cells per donor. A Mann-Whitney test was used to compare the two cell populations. *: p value < 0.05; ****: p value < 0.0001.

decreased when substrate rigidity increases. It would mean that macrophages' ability to phagocytose would be lessened in stiff environments, such as fibrotic tissues; that effect could contribute to disease progression. Reports in the literature on this question have been conflicting, with studies finding that substrate stiffness had no effect on phagocytosis[23] or only after LPS treatment,[26] and other studies reporting opposite effects of substrate stiffness on phagocytic uptake.[27–29] Differences in experimental conditions, especially the range of substrate elastic moduli tested and the properties of the phagocytic targets used, appear critical to understand this lack of consistency. Importantly, however, no mechanism has been proposed to explain the effect of substrate stiffness on internalization in these studies. In our case, differences in initial target capture and CR3 activation state were not enough to fully explain the differences in phagocytic uptake. A possible explanation would be to take into account how the actin cytoskeleton is organized in macrophages prior to a challenge with phagocytic targets. Work on retinal pigment epithelial cells, whose ability to phagocytose fragments shed by photoreceptor cells is critical for normal vision, showed that the presence of a high number of F-actin stress fibers in these cells decreased their capacity to bind and internalize phagocytic targets.[30] Similarly, as macrophages formed fewer podosomes on soft substrates, F-actin could be better mobilized during phagocytosis on these surfaces and lead to better particle uptake. This hypothesis would be consistent with our results on the effect of substrate stiffness on F-actin recruitment during phagocytosis. Several studies have also shown that cell adhesion increases plasma membrane tension,[31,32] and a recent study reported that neutrophils with an

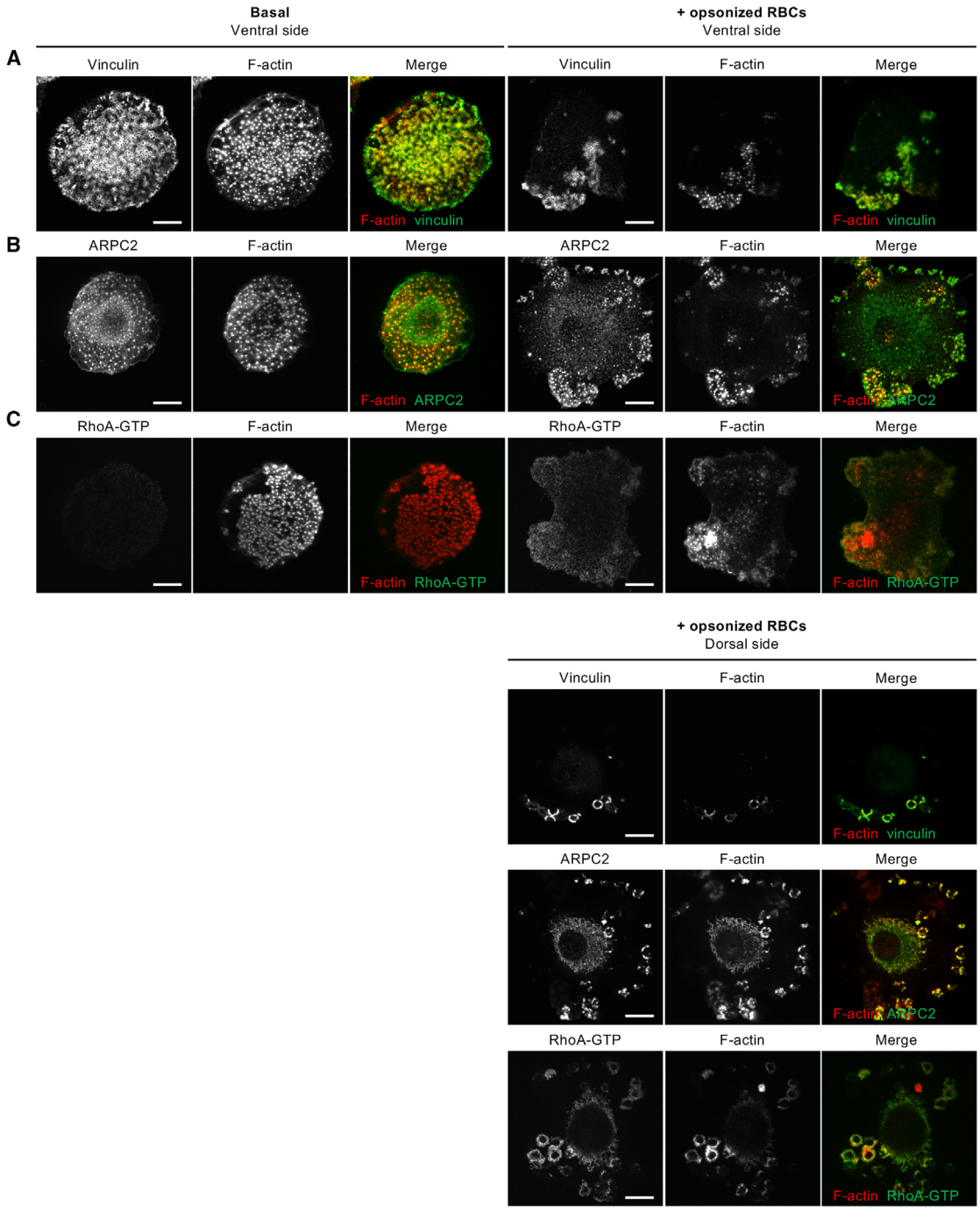

Figure 6. Relocalization of proteins associated with podosomes or phagocytic cups during integrin-mediated phagocytosis

hMDMs were seeded on glass coverslips, incubated at 37°C for 4 h and challenged with opsonized RBCs. Cells were fixed at steady state (basal) or after a 2-min incubation with RBCs, permeabilized and labeled with Alexa Fluor 488-conjugated phalloidin and a mouse antibody that recognizes vinculin (A), rabbit antibodies against p34-Arc/ARPC2 (B) or a recombinant antibody that recognizes RhoA-GTP (C), followed by Alexa Fluor 647-labeled anti-mouse, anti-rabbit or anti-human IgG antibodies. Representative confocal images of the ventral side (upper panel) or dorsal side (lower panel) of macrophages at steady state (left) or during phagocytosis of opsonized RBCs (right). On merge images, F-actin is shown in red and vinculin, ARPC2 or RhoA-GTP is shown in green. Scale bar, 10 μm.

excess of plasma membrane and lower membrane tension are able to phagocytose a higher number of particles.[33] We could then imagine that macrophages with fewer podosomes on soft surfaces could have decreased membrane tension compared to their counterparts on stiff surfaces, which would facilitate the formation of protrusions around phagocytic targets. In

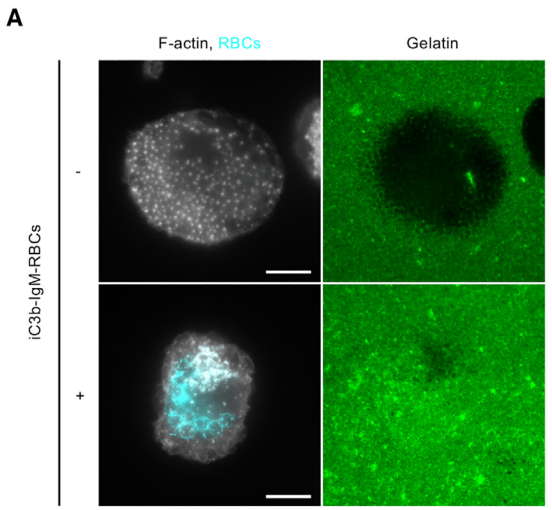

Figure 7. Integrin-mediated phagocytosis decreases gelatin degradation by macrophages

hMDMs were seeded on fluorescent gelatin-coated coverslips and incubated at 37°C for 1 h and challenged with opsonized RBCs (iC3b-IgM-RBCs). Cells were fixed after 2 h, permeabilized and labeled with Alexa Fluor 633-conjugated phalloidin and Cy3-labeled anti-rabbit antibodies that recognize the anti-sheep RBCs IgMs used to opsonize RBCs.

(A) Representative wide-field images of macrophages challenged (lower panel) or not (upper panel) with RBCs. F-actin is shown in gray, RBCs in cyan and gelatin in green. Scale bar, 10 μm.

(B) Quantification of mean degradation area per cell. Each dot corresponds to the mean of at least 30 cells per condition and per donor. A ratio paired t test was used to compare the means of all 4 donors. *: p value < 0.05.

support of this idea, an effect of adhesiveness on macropinocytosis was recently described in macrophages.[34] These hypotheses do not explain the phenotype observed on glass coverslips, but the physical properties of glass make these surfaces big outliers when compared to the polyacrylamide gels. Overall, our results and those of others indicate that substrate properties do have an important effect on phagocytic uptake, but the relative contributions of macrophage prior activation, substrate stiffness, type of phagocytic receptor(s) engaged, and physical properties of the target are still not well understood.

We then asked if, conversely, phagocytosis has an effect on the way macrophages interact with their environment. We found that CR3-mediated phagocytosis led to a transient loss of podosomes on the ventral side of macrophages, at the same time as F-actin recruitment around targets at phagocytic cups. Other proteins characteristic of macrophage podosomes, such as vinculin and ARPC2, were also lost from the ventral side of macrophages and recruited at phagocytic cups concomitantly with F-actin. While many studies (reviewed by Linder and Barcelona[35]) have described actin structures at phagocytic cups referred to as "podosome-like" given their similarities with podosomes in terms of composition and organization, the consequences of phagocytic receptor engagement on podosome dynamics has not been extensively described. Observations similar to ours were made in a previous study of phagocytosis mediated by a different receptor, the Fcγ receptor.[36] Of note, as CR3 is also involved in phagocytosis of IgG-opsonized particles,[37,38] similar mechanisms could be at play in both types of phagocytosis. This active remodeling of macrophage adhesion during phagocytosis is consistent with the fact that phagocytosing macrophages interact more dynamically with substrate, as found by traction force microscopy.

As they involve many of the same molecular actors, inhibiting one process (phagocytosis or podosome dynamics) by a drug or protein depletion often inhibits the other one as well, which makes the study of the underlying mechanisms challenging. Several hypotheses can nonetheless be brought forward: first, podosome disruption could be triggered by signaling induced downstream of phagocytic receptor engagement. In support of this idea, the RhoA-ROCK-myosin IIA pathway, which is crucial to drive CR3-mediated phagocytosis,[19,39] was found to be responsible for podosome dissolution in response to PGE2 in dendritic cells.[40] RhoA was also responsible for podosome loss after phagocytosis of IgG-opsonized particles, but the observed podosome disruption occurred following phagosome maturation in that case, suggesting that several pathways can link phagocytosis with podosome dynamics.[41] Podosome disruption could also be a direct consequence of the recruitment of F-actin and other proteins at the dorsal side of macrophages, effectively depleting them from the ventral side. It could also be explained by a competition for effectors between actors involved in podosome formation, on the one hand, and phagocytosis, on the other hand; for example, between RhoA, which is the small GTPase from the Rho family whose role is most important to induce F-actin reorganization during CR3-mediated phagocytosis, and Cdc42, which mediates branched F-actin polymerization in podosomes.[21] Lastly, the loss of podosomes could involve physical constraints on the plasma membrane during phagocytosis. Several studies have reported an increase in plasma membrane tension during phagocytosis[42,43] and podosome dynamics were found to be modulated by factors affecting membrane tension, independently of actomyosin contraction.[44]

We show that there is a connection between what happens at the dorsal side of macrophages (phagocytosis) and at their ventral side (adhesion and matrix degradation), involving a dynamic actin remodeling. *In vivo*, this type of crosstalk might be critical for innate immune cells to shift from a still sentinel function to a more dynamic sampling and scavenging activity.

Limitations of the study

This work presents several limitations that are inherent to the study of cell behavior *in vitro*. Macrophages were seeded either on glass or on hydrogels composed of polyacrylamide; these substrates do not accurately recapitulate the 3D environment

in which macrophages can be found in an organism. In addition, while this study used exclusively monocyte-derived primary macrophages and not a macrophage cell line, these cells still differ significantly from tissue-resident macrophages because of the lack of tissue- and niche-specific cues that macrophages rely on *in vivo*. Finally, we were limited in our study of the cross-talk between adhesion and phagocytosis in macrophages as these two cell functions involve many of the same molecular actors; targeting these actors therefore inhibited both processes.

RESOURCE AVAILABILITY

Lead contact

Requests for further information and resources should be directed to and will be fulfilled by the lead contact, Dr. Florence Niedergang (florence.niedergang@inserm.fr).

Materials availability

This study did not generate new unique reagents.

Data and code availability

All data reported in this paper will be shared by the lead contact upon request. This paper does not report original code. Any additional information required to reanalyze the data reported in this paper is available from the lead contact upon request.

ACKNOWLEDGMENTS

We thank Dr. David Remy and Dr. Philippe Chavrier for their kind help in setting up gelatin degradation experiments. We thank the IMAG'IC facility of Institut Cochin that is part of the national France-BioImaging infrastructure supported by Agence Nationale de la Recherche (ANR-10-INBS-04). Work in the laboratory of F.N. was supported by grants from CNRS, Inserm, Université Paris Descartes (now Université Paris Cité), and Agence Nationale de la Recherche (ANR 16-CE13-0007-01, ANR 20-CE13-0017-01) that included A.M.'s salary. M.D. was supported by a PhD fellowship from the French Ministry of Higher Education, Research and Innovation and by a fellowship from Fondation pour la Recherche Médicale (FRM; FDT202304016443). Work in the laboratory of M.B. was supported by Agence Nationale de la Recherche (ANR-17-CE30–0032-01 and ANR-21-CE13-0042-02 for A.R.'s salary).

AUTHOR CONTRIBUTIONS

M.D., conceptualization, formal analysis, investigation, methodology, validation, visualization, writing – original draft, and writing – review and editing; A.M., conceptualization, formal analysis, investigation, methodology, validation, visualization, writing – original draft, and writing – review and editing; A.R., conceptualization, formal analysis, methodology, validation, visualization, and writing – original draft; C.L.C., conceptualization, funding acquisition, methodology, validation, and writing – review and editing; M.B., conceptualization, formal analysis, funding acquisition, investigation, methodology, supervision, validation, visualization, and writing – original draft; F.N., conceptualization, formal analysis, funding acquisition, investigation, methodology, supervision, validation, visualization, writing – original draft, and writing – review and editing.

DECLARATION OF INTERESTS

The authors declare no competing interests.

STAR★METHODS

Detailed methods are provided in the online version of this paper and include the following:

SUPPLEMENTAL INFORMATION

Supplemental information can be found online at https://doi.org/10.1016/j.isci.2025.112067.

Received: August 16, 2024
Revised: October 25, 2024
Accepted: February 17, 2025
Published: February 20, 2025

REFERENCES

1. Uribe-Querol, E., and Rosales, C. (2020). Phagocytosis: Our Current Understanding of a Universal Biological Process. Front. Immunol. *11*, 1066. https://doi.org/10.3389/fimmu.2020.01066.
2. Depierre, M., Jacquelin, L., and Niedergang, F. (2023). Phagocytosis. In Encyclopedia of Cell Biology, A. Bradshaw Ralph, W. Hart Gerald, and D. Stahl Philip, eds. (Oxford: Elsevier), pp. 286–295.
3. Torres-Gomez, A., Cabañas, C., and Lafuente, E.M. (2020). Phagocytic Integrins: Activation and Signaling. Front. Immunol. *11*, 738. https://doi.org/10.3389/fimmu.2020.00738.
4. Doran, A.C., Yurdagul, A., Jr., and Tabas, I. (2020). Efferocytosis in health and disease. Nat. Rev. Immunol. *20*, 254–267. https://doi.org/10.1038/s41577-019-0240-6.
5. Mass, E., Nimmerjahn, F., Kierdorf, K., and Schlitzer, A. (2023). Tissue-specific macrophages: how they develop and choreograph tissue biology. Nat. Rev. Immunol. *23*, 563–579. https://doi.org/10.1038/s41577-023-00848-y.
6. Butcher, D.T., Alliston, T., and Weaver, V.M. (2009). A tense situation: forcing tumour progression. Nat. Rev. Cancer *9*, 108–122. https://doi.org/10.1038/nrc2544.
7. Cox, T.R., and Erler, J.T. (2011). Remodeling and homeostasis of the extracellular matrix: implications for fibrotic diseases and cancer. Dis. Model. Mech. *4*, 165–178. https://doi.org/10.1242/dmm.004077.
8. Medzhitov, R. (2008). Origin and physiological roles of inflammation. Nature *454*, 428–435. https://doi.org/10.1038/nature07201.
9. Paszek, M.J., Zahir, N., Johnson, K.R., Lakins, J.N., Rozenberg, G.I., Gefen, A., Reinhart-King, C.A., Margulies, S.S., Dembo, M., Boettiger, D., et al. (2005). Tensional homeostasis and the malignant phenotype. Cancer Cell *8*, 241–254. https://doi.org/10.1016/j.ccr.2005.08.010.
10. Du, H., Bartleson, J.M., Butenko, S., Alonso, V., Liu, W.F., Winer, D.A., and Butte, M.J. (2023). Tuning immunity through tissue mechanotransduction. Nat. Rev. Immunol. *23*, 174–188. https://doi.org/10.1038/s41577-022-00761-w.
11. Meli, V.S., Veerasubramanian, P.K., Atcha, H., Reitz, Z., Downing, T.L., and Liu, W.F. (2019). Biophysical regulation of macrophages in health

and disease. J. Leukoc. Biol. *106*, 283–299. https://doi.org/10.1002/JLB.MR0318-126R.

12. Previtera, M.L., and Sengupta, A. (2015). Substrate Stiffness Regulates Proinflammatory Mediator Production through TLR4 Activity in Macrophages. PLoS One *10*, e0145813. https://doi.org/10.1371/journal.pone.0145813.
13. Meli, V.S., Atcha, H., Veerasubramanian, P.K., Nagalla, R.R., Luu, T.U., Chen, E.Y., Guerrero-Juarez, C.F., Yamaga, K., Pandori, W., Hsieh, J.Y., et al. (2020). YAP-mediated mechanotransduction tunes the macrophage inflammatory response. Sci. Adv. *6*, eabb8471. https://doi.org/10.1126/sciadv.abb8471.
14. Jaumouille, V., and Waterman, C.M. (2020). Physical Constraints and Forces Involved in Phagocytosis. Front. Immunol. *11*, 1097. https://doi.org/10.3389/fimmu.2020.01097.
15. Vorselen, D., Labitigan, R.L.D., and Theriot, J.A. (2020). A mechanical perspective on phagocytic cup formation. Curr. Opin. Cell Biol. *66*, 112–122. https://doi.org/10.1016/j.ceb.2020.05.011.
16. Discher, D.E., Janmey, P., and Wang, Y.L. (2005). Tissue cells feel and respond to the stiffness of their substrate. Science *310*, 1139–1143. https://doi.org/10.1126/science.1116995.
17. Handorf, A.M., Zhou, Y., Halanski, M.A., and Li, W.J. (2015). Tissue stiffness dictates development, homeostasis, and disease progression. Organogenesis *11*, 1–15. https://doi.org/10.1080/15476278.2015.1019687.
18. Linder, S., and Wiesner, C. (2015). Tools of the trade: podosomes as multipurpose organelles of monocytic cells. Cell. Mol. Life Sci. *72*, 121–135. https://doi.org/10.1007/s00018-014-1731-z.
19. Caron, E., and Hall, A. (1998). Identification of two distinct mechanisms of phagocytosis controlled by different Rho GTPases. Science *282*, 1717–1721. https://doi.org/10.1126/science.282.5394.1717.
20. Wiedemann, A., Patel, J.C., Lim, J., Tsun, A., van Kooyk, Y., and Caron, E. (2006). Two distinct cytoplasmic regions of the beta2 integrin chain regulate RhoA function during phagocytosis. J. Cell Biol. *172*, 1069–1079. https://doi.org/10.1083/jcb.200508075.
21. Linder, S., Cervero, P., Eddy, R., and Condeelis, J. (2023). Mechanisms and roles of podosomes and invadopodia. Nat. Rev. Mol. Cell Biol. *24*, 86–106. https://doi.org/10.1038/s41580-022-00530-6.
22. Fereol, S., Fodil, R., Labat, B., Galiacy, S., Laurent, V.M., Louis, B., Isabey, D., and Planus, E. (2006). Sensitivity of alveolar macrophages to substrate mechanical and adhesive properties. Cell Motil Cytoskeleton *63*, 321–340. https://doi.org/10.1002/cm.20130.
23. Adlerz, K.M., Aranda-Espinoza, H., and Hayenga, H.N. (2016). Substrate elasticity regulates the behavior of human monocyte-derived macrophages. Eur. Biophys. J. *45*, 301–309. https://doi.org/10.1007/s00249-015-1096-8.
24. Labernadie, A., Bouissou, A., Delobelle, P., Balor, S., Voituriez, R., Proag, A., Fourquaux, I., Thibault, C., Vieu, C., Poincloux, R., et al. (2014). Protrusion force microscopy reveals oscillatory force generation and mechanosensing activity of human macrophage podosomes. Nat. Commun. *5*, 5343. https://doi.org/10.1038/ncomms6343.
25. Linder, S., and Wiesner, C. (2016). Feel the force: Podosomes in mechanosensing. Exp. Cell Res. *343*, 67–72. https://doi.org/10.1016/j.yexcr.2015.11.026.
26. Scheraga, R.G., Abraham, S., Niese, K.A., Southern, B.D., Grove, L.M., Hite, R.D., McDonald, C., Hamilton, T.A., and Olman, M.A. (2016). TRPV4 Mechanosensitive Ion Channel Regulates Lipopolysaccharide-Stimulated Macrophage Phagocytosis. J. Immunol. *196*, 428–436. https://doi.org/10.4049/jimmunol.1501688.
27. Patel, N.R., Bole, M., Chen, C., Hardin, C.C., Kho, A.T., Mih, J., Deng, L., Butler, J., Tschumperlin, D., Fredberg, J.J., et al. (2012). Cell elasticity determines macrophage function. PLoS One *7*, e41024. https://doi.org/10.1371/journal.pone.0041024.
28. Sridharan, R., Cavanagh, B., Cameron, A.R., Kelly, D.J., and O'Brien, F.J. (2019). Material stiffness influences the polarization state, function and migration mode of macrophages. Acta Biomater. *89*, 47–59. https://doi.org/10.1016/j.actbio.2019.02.048.
29. Kalashnikov, N., and Moraes, C. (2023). Substrate viscoelasticity affects human macrophage morphology and phagocytosis. Soft Matter *19*, 2438–2445. https://doi.org/10.1039/d2sm01683d.
30. Muller, C., Charniga, C., Temple, S., and Finnemann, S.C. (2018). Quantified F-Actin Morphology Is Predictive of Phagocytic Capacity of Stem Cell-Derived Retinal Pigment Epithelium. Stem Cell Rep. *10*, 1075–1087. https://doi.org/10.1016/j.stemcr.2018.01.017.
31. Lieber, A.D., Yehudai-Resheff, S., Barnhart, E.L., Theriot, J.A., and Keren, K. (2013). Membrane tension in rapidly moving cells is determined by cytoskeletal forces. Curr. Biol. *23*, 1409–1417. https://doi.org/10.1016/j.cub.2013.05.063.
32. Sakamoto, R., Banerjee, D.S., Yadav, V., Chen, S., Gardel, M.L., Sykes, C., Banerjee, S., and Murrell, M.P. (2023). Membrane tension induces F-actin reorganization and flow in a biomimetic model cortex. Commun. Biol. *6*, 325. https://doi.org/10.1038/s42003-023-04684-7.
33. Winer, B.Y., Settle, A.H., Yakimov, A.M., Jeronimo, C., Lazarov, T., Tipping, M., Saoi, M., Sawh, A., Sepp, A.L.L., Galiano, M., et al. (2024). Plasma membrane abundance dictates phagocytic capacity and functional cross-talk in myeloid cells. Sci. Immunol. *9*, eadl2388. https://doi.org/10.1126/sciimmunol.adl2388.
34. Renkawitz, J., Braun, M., Reza, R., Kameritsch, P., Ruiz-Fernandez, M., Schmitt, M., Shnipova, M., Krug, A., Merrin, J., and Polleux, J. (2024). Microenvironmental regulation of macropinocytosis facilitates extracellular fluid sampling. Preprint at Res. Sq. https://doi.org/10.21203/rs.3.rs-4223901/v1.
35. Linder, S., and Barcelona, B. (2023). Get a grip: Podosomes as potential players in phagocytosis. Eur. J. Cell Biol. *102*, 151356. https://doi.org/10.1016/j.ejcb.2023.151356.
36. Tertrais, M., Bigot, C., Martin, E., Poincloux, R., Labrousse, A., and Maridonneau-Parini, I. (2021). Phagocytosis is coupled to the formation of phagosome-associated podosomes and a transient disruption of podosomes in human macrophages. Eur. J. Cell Biol. *100*, 151161. https://doi.org/10.1016/j.ejcb.2021.151161.
37. Jongstra-Bilen, J., Harrison, R., and Grinstein, S. (2003). Fcgamma-receptors induce Mac-1 (CD11b/CD18) mobilization and accumulation in the phagocytic cup for optimal phagocytosis. J. Biol. Chem. *278*, 45720–45729. https://doi.org/10.1074/jbc.M303704200.
38. Freeman, S.A., Goyette, J., Furuya, W., Woods, E.C., Bertozzi, C.R., Bergmeier, W., Hinz, B., van der Merwe, P.A., Das, R., and Grinstein, S. (2016). Integrins Form an Expanding Diffusional Barrier that Coordinates Phagocytosis. Cell *164*, 128–140. https://doi.org/10.1016/j.cell.2015.11.048.
39. Olazabal, I.M., Caron, E., May, R.C., Schilling, K., Knecht, D.A., and Machesky, L.M. (2002). Rho-kinase and myosin-II control phagocytic cup formation during CR, but not FcgammaR, phagocytosis. Curr. Biol. *12*, 1413–1418. https://doi.org/10.1016/s0960-9822(02)01069-2.
40. van Helden, S.F.G., Oud, M.M., Joosten, B., Peterse, N., Figdor, C.G., and van Leeuwen, F.N. (2008). PGE2-mediated podosome loss in dendritic cells is dependent on actomyosin contraction downstream of the RhoA-Rho-kinase axis. J. Cell Sci. *121*, 1096–1106. https://doi.org/10.1242/jcs.020289.
41. Ferling, I., Pfalzgraf, S., Moutounet, L., Qiu, L., Li, I., Zhou, Y., Grinstein, S., and Freeman, S.A. (2024). https://doi.org/10.1101/2024.01.31.578237.
42. Masters, T.A., Pontes, B., Viasnoff, V., Li, Y., and Gauthier, N.C. (2013). Plasma membrane tension orchestrates membrane trafficking, cytoskeletal remodeling, and biochemical signaling during phagocytosis. Proc. Natl. Acad. Sci. USA *110*, 11875–11880. https://doi.org/10.1073/pnas.1301766110.
43. Barger, S.R., Reilly, N.S., Shutova, M.S., Li, Q., Maiuri, P., Heddleston, J.M., Mooseker, M.S., Flavell, R.A., Svitkina, T., Oakes, P.W., et al.

(2019). Membrane-cytoskeletal crosstalk mediated by myosin-I regulates adhesion turnover during phagocytosis. Nat. Commun. *10*, 1249. https://doi.org/10.1038/s41467-019-09104-1.

44. Rafiq, N.B.M., Grenci, G., Lim, C.K., Kozlov, M.M., Jones, G.E., Viasnoff, V., and Bershadsky, A.D. (2019). Forces and constraints controlling podosome assembly and disassembly. Philos. Trans. R. Soc. Lond. B Biol. Sci. *374*, 20180228. https://doi.org/10.1098/rstb.2018.0228.
45. Remy, D., Macé, A.S., Chavrier, P., and Monteiro, P. (2023). Invadopodia Methods: Detection of Invadopodia Formation and Activity in Cancer Cells Using Reconstituted 2D and 3D Collagen-Based Matrices. Methods Mol. Biol. *2608*, 225–246. https://doi.org/10.1007/978-1-0716-2887-4_14.
46. Tse, J.R., and Engler, A.J. (2010). Preparation of hydrogel substrates with tunable mechanical properties. Curr. Protoc. Cell Biol. *47*, 10–16, Unit 10 16. https://doi.org/10.1002/0471143030.cb1016s47.
47. Gross, W., and Kress, H. (2017). Simultaneous measurement of the Young's modulus and the Poisson ratio of thin elastic layers. Soft Matter *13*, 1048–1055. https://doi.org/10.1039/c6sm02470j.

STAR★METHODS

KEY RESOURCES TABLE

REAGENT or RESOURCE	SOURCE	IDENTIFIER
Antibodies		
Anti-vinculin (clone hVIN-1)	Sigma-Aldrich (Merck)	Cat#V9131; RRID: AB_477629
Anti-p34-Arc/ARPC2	Sigma-Aldrich (Merck)	Cat#07-227; RRID: AB_11212539
Anti-sheep red blood cells (RBCs) rabbit IgMs	Gentaur	Cat#MBS524107
Anti-RhoA-GTP	CurieCoreTech recombinant antibody facility (Institut Curie)	Cat#A-R-H#62
Alexa Fluor 647-labeled F(ab')$_2$ donkey anti-mouse IgG (H+L)	Jackson ImmunoResearch	Cat#715-606-150; RRID: AB_2340865
Cy3-labeled F(ab')$_2$ donkey anti-rabbit IgG (H+L)	Jackson ImmunoResearch	Cat#711-166-152; RRID: AB_2313568
Alexa Fluor 647-labeled F(ab')$_2$ donkey anti-rabbit IgG (H+L)	Jackson ImmunoResearch	Cat#711-606-152; RRID: AB_2340625
Alexa Fluor 647-labeled F(ab')$_2$ goat anti-human IgG (H+L)	Jackson ImmunoResearch	Cat#109-606-088; RRID: AB_2337897
Biological samples		
Complement C5-deficient human serum	Sigma-Aldrich (Merck)	Cat#C1163
Human blood from healthy donors (apheresis cassettes)	Etablissement Français du Sang (EFS)	INSERM agreement 18/EFS/030 and CNRS agreement 2023-2026-025 CCPSL CNRS
Chemicals, peptides, and recombinant proteins		
Phorbol 12-myristate 13-acetate (PMA)	Sigma-Aldrich (Merck)	Cat#P1585
4',6-diamidino-2-phenylindole (DAPI)	Sigma-Aldrich (Merck)	Cat#D9542
Phalloidin Alexa Fluor 488	Invitrogen	Cat#A12379
Phalloidin Alexa Fluor 633	Invitrogen	Cat#A22284
Ficoll-Paque Plus	Merck	Cat#GE17-1440-03
Percoll	Sigma-Aldrich (Merck)	Cat#GE17-0891-01
Human GM-CSF	Miltenyi	Cat#130-093-865
Human M-CSF	Miltenyi	Cat#130-096-491
Acrylamide	Sigma-Aldrich (Merck)	Cat#A4058
Bis-acrylamide	Sigma-Aldrich (Merck)	Cat#M1533
Paraformaldehyde	Electron Microscopy Sciences	Cat#19210
Glutaraldehyde	Electron Microscopy Sciences	Cat#16200
Poly-L-lysine	Sigma-Aldrich (Merck)	Cat#P8920
Fluoromount-G	Interchim	Cat#FP-483331
Software and algorithms		
Prism v9.3.1	GraphPad	https://www.graphpad.com/
Fiji v2.0.0-rc-69/1.52p	U.S. National Institutes of Health	https://imagej.net/software/fiji/
Other		
Softslip Easy Coat hydrogels bound to 12-mm #1 glass coverslips, 4 kPa	Matrigen	Cat#SS24-EC-4-EA
Softslip Easy Coat hydrogels bound to 12-mm #1 glass coverslips, 12 kPa	Matrigen	Cat#SS24-EC-12-EA
Softslip Easy Coat hydrogels bound to 12-mm #1 glass coverslips, 25 kPa	Matrigen	Cat#SS24-EC-25-EA
Fetal bovine serum	Life Technologies	Cat#10270106
Sheep blood in Alsevers	Rockland Immunochemicals	Cat#R311-0050

(*Continued on next page*)

Continued

REAGENT or RESOURCE	SOURCE	IDENTIFIER
Gelatin Oregon Green 488	Invitrogen	Cat#G13186
Fibronectin	Sigma-Aldrich (Merck)	Cat#F1141
Saponin	Sigma-Aldrich (Merck)	Cat#S7900
35-mm glass-bottom cell culture dishes	MatTek	Cat#P35G-0-14-C
FluoSpheres carboxylate-modified microspheres	Invitrogen	Cat#F8810

EXPERIMENTAL MODEL AND STUDY PARTICIPANT DETAILS

Primary cultures of human macrophages

Primary human macrophages were differentiated from monocytes isolated from the blood of healthy donors, obtained from the Établissement Français du Sang, in agreement with INSERM (18/EFS/030) and CNRS (2023-2026-025 CCPSL CNRS). Written consent was given by all donors and samples were anonymized (no information was provided on the age and sex of the donors).

METHOD DETAILS

Antibodies and reagents

Phorbol 12-myristate 13-acetate (PMA) (P1585), complement C5-deficient human serum (C1163), anti-vinculin (clone hVIN-1) (V9131), anti-p34-Arc/ARPC2 (07-227) and DAPI (2-(4-amidinophenyl)-1*H*-indole-6-carboxamidine) (D9542) were obtained from Merck. Anti-RhoA-GTP was from the CurieCoreTech recombinant antibody facility (Institut Curie). Anti-sheep red blood cells (RBCs) rabbit IgMs were obtained from Gentaur (MBS524107). Phalloidin conjugated to Alexa Fluor 488 (A12379) or Alexa Fluor 633 (A22284) was purchased from Invitrogen. Alexa Fluor 488, Alexa Fluor 647 or Cy3-labeled $F(ab')_2$ anti-mouse, anti-human or anti-rabbit IgG (H+L) were obtained from Jackson ImmunoResearch.

Cell culture

Human blood of healthy donors was obtained from the Établissement Français du Sang (INSERM agreement 18/EFS/030 and CNRS agreement 2023-2026-025 CCPSL CNRS). All donors gave written informed consent and samples were anonymized. Blood samples were diluted 1:1 in PBS 1 mM EDTA and peripheral blood mononuclear cells (PBMCs) were isolated by Ficoll-Paque (Merck, GE17-1440-03) density gradient centrifugation. Lymphocytes were eliminated by a 56% Percoll (Sigma-Aldrich, GE17-0891-01) density gradient centrifugation. The remaining cells (monocytes) were seeded in R10 medium (RPMI 1640 with GlutaMAX (Gibco, 61870-010) supplemented with 10% fetal bovine serum (FBS, Life Technologies, 10270106), 10 mM HEPES (Gibco, 15630080), 1 mM sodium pyruvate (Gibco, 11360039), 1X non-essential amino acids (Gibco, 11140035) and 100 μg/mL penicillin/streptomycin (Gibco, 15140122)) with 4 ng/mL GM-CSF (Miltenyi, 130-093-865) and 0.5 ng/mL M-CSF (Miltenyi, 130-096-491). Medium and cytokines were renewed on day 3 or 4 of differentiation. On day 7, medium was replaced by macrophage medium (RPMI 1640 with GlutaMAX (Gibco, 61870-010) supplemented with 10% fetal bovine serum (FBS, Life Technologies, 10270106), 2 mM L-glutamine (Gibco, 25030024) and 100 μg/mL penicillin/streptomycin (Gibco, 15140122)). Monocyte-derived macrophages were used for experiments from day 8 to day 12 of differentiation. Cells were detached from cell culture plates by incubating them in PBS 1X, 2 mM EDTA for 40 min at 4°C, washed once with PBS 1X then resuspended in macrophage medium and seeded at a density of 2.5 x 10^4 cells per cm^2.

Complement-mediated phagocytosis assay

Sheep RBCs purified from sheep blood (Rockland, R311-0050) were used as phagocytic targets. RBCs were opsonized to target CR3 as follows: after being washed twice in PBS 1X 0.1% BSA (bovine serum albumin, Euromedex 04-100-812-E), RBCs were incubated with rabbit IgM anti-sheep RBCs (Gentaur, MBS524107) at 1/80 in PBS 1X 0.1% BSA for 30 min at room temperature. RBCs were again washed in PBS 1X 0.1% BSA and incubated in phagocytosis medium (RPMI 1640 with GlutaMAX (Gibco, 61870-010) supplemented with 2 mM L-glutamine (Gibco, 25030024) and 100 μg/mL penicillin/streptomycin (Gibco, 15140122)) containing 10% of complement C5-deficient human serum (Merck, C1163) for 20 min at 37°C. Opsonized RBCs (iC3b-IgM-RBCs) were then resuspended in pre-warmed phagocytosis medium. Alternatively, the incubation step with IgM was skipped and RBCs were opsonized only with 10% complement C5-deficient serum (iC3b-RBCs). When mentioned, macrophages were pretreated with 150 ng/mL PMA in phagocytosis medium for 15 min at 37°C prior to adding RBCs. Phagocytosis was initiated by distributing the RBCs on macrophages and synchronization was ensured by centrifuging the cells at 500 g for 2 min. Cells were then placed back in the incubator at 37°C, 5% CO_2 for the indicated time periods.

Hydrogels

Polyacrylamide hydrogels bound to glass coverslips (Softslip Easy Coat hydrogels, bound to 12-mm #1 glass coverslips, SS24-EC-4-EA (4 kPa), SS24-EC-12-EA (12 kPa) or SS24-EC-25-EA (25 kPa)) were purchased from Matrigen to compare phagocytosis on substrates of varying stiffnesses. Hydrogels were incubated with 10 μg/mL fibronectin (Merck, F1141) diluted in PBS 1X for 1 h at room temperature or, alternatively, overnight at 4°C. Hydrogels were then rinsed once with PBS 1X and once with macrophage medium prior to adding the differentiated macrophages. They were allowed to re-adhere for 4 h at 37°C, 5% CO_2.

Fluorescent gelatin degradation assay

Fluorescent gelatin-coated coverslips were prepared as described in Remy et al.[45] Briefly, glass coverslips were coated with poly-L-lysine (Sigma-Aldrich, P8920) at 10 μg/mL in H_2O for 20 min at room temperature, rinsed with H_2O and treated with 0.5% glutaraldehyde (Electron Microscopy Science, 16200) in PBS 1X for 10 min. After three rinses with PBS 1X, the coverslips were coated with gelatin coupled to Oregon Green 488 (Invitrogen, G13186) resuspended at 0.2 mg/mL in 2% sucrose for 10 min at room temperature and rinsed with PBS 1X before being treated with 133 mM sodium borohydride in PBS 1X for 3 min. The coverslips were finally rinsed three times with PBS 1X and stored at 4°C until use. Macrophages were allowed to re-adhere on these coverslips for 1 h before being challenged with iC3b-IgM-RBCs for 2 h at 37°C, 5% CO_2.

Immunofluorescence microscopy

Cells were fixed in 4% paraformaldehyde (Electron Microscopy Sciences, 19210) in PBS 1X for 15 min at room temperature and quenched for 10 min with 50 mM NH_4Cl in PBS 1X. Coverslips were then washed once in PBS 1X and incubated in PBS 1X, 2% FBS, 0.05% saponin (Sigma-Aldrich, S7900) (permeabilization buffer) for 10 to 15 min. Coverslips were incubated with primary antibodies diluted in permeabilization buffer for 45 min at room temperature, washed three times then incubated with secondary antibodies, fluorescent phalloidin and DAPI in permeabilization buffer for 30 min at room temperature. After three washes, coverslips were mounted onto slides with Fluoromount-G (Interchim, FP-483331).

Images were acquired using an inverted wide-field microscope (Leica DMI6000) with a 100× (1.4 NA) HCX APO oil-immersion objective, an ORCA flash 4 LT camera (Hamamatsu) and a HXP R 120W/45C VIS lamp. This system was controlled using the Metamorph software (Molecular Devices). Image acquisitions were also performed using a spinning disk confocal microscope (Yokogawa CSU-W1 T1) with a 100× (1.4 NA) PLAN APO CHROME oil-immersion objective, an ORCA sCMOS flash 4.0 v3 camera (Hamamatsu) and OBIS lasers (Coherent). That system was controlled using the cellSens software (Olympus). A z-stack series of images was taken every 0.25 μm.

Quantitative analysis of phagocytic uptake

Internalized RBCs were defined as particles positive for the fluorescent labeling with the fluorescent $F(ab')_2$ anti-rabbit IgG and detected by phase contrast as holes in the cells. External RBCs were associated with a cell and positive for the fluorescent labeling but not detected by phase contrast. The number of cell-associated (bound + internalized) and the number of internalized RBCs were counted in 25-30 cells chosen at random on the coverslips. Phagocytosis efficiency was calculated as the percentage of bound RBCs that were internalized.

Fluorescence image analysis

Images were analyzed with Fiji (U.S. National Institutes of Health). Cell spreading area was measured on the plane closest to the coverslip based on the F-actin staining. Podosomes were detected using the "Maximum Entropy" threshold plugin on Fiji, only considering regions > 10 pixels and whose circularity was comprised between 0.5 and 1. The number of podosome was then divided by the cell spreading area to obtain the podosome density. A homemade macro for this quantification was created on Fiji and is available upon request.

For quantification of gelatin degradation, the total area of degradation (darker pixels) was measured with the threshold command of ImageJ. The total degradation area was then divided by the number of cells to obtain the mean degradation area per cell.

Substrate preparation and characterization for traction force microscopy

10 kPa polyacrylamide gels for traction force microscopy were prepared as described in Tse and Engler.[46] Briefly, 10% acrylamide (Sigma-Aldrich, A4058) and 0.1% bis-acrylamide (Sigma-Aldrich, M1533) solution containing 200 nm fluorescent beads (Invitrogen, F8810) was allowed to polymerize between plasma-cleaned, fibronectin-coated (Merck, F1141), 12-mm diameter coverslips and silanized glass-bottom cell culture dishes (MatTek, P35G-0-14-C). Resulting gels had a thickness of 60-100 nm and it was verified that the method reliably yielded gels with stiffnesses within the error range provided by Tse and Engler using the method of Gross and Kress.[47]

Traction force microscopy

Macrophages were allowed to re-adhere to fibronectin-coated 10 kPa polyacrylamide gels described above for 4 h. Imaging was performed at 37°C, 5% CO_2 using an inverted wide-field microscope (iMIC TILL Photonics) with a 60× (1.49 NA) ApoN TIRFM objective and an EMCCD camera (ANDOR technology). Cells were observed with brightfield illumination for at least 30 min in phagocytosis

medium, in the case of control cells, or medium containing iC3b-IgM-RBCs, to serve as phagocytic targets for phagocytosing cells. Simultaneous fluorescence images of fluorescent beads in the surface plane of the gel were acquired for calculation of traction forces. Images were acquired every 10 s. The calculation method has been described in detail elsewhere (Mandal et al., 2014). Briefly, bead images were corrected for drift and then divided into 19 μm^2 sub-images. Single particle tracking was performed in each sub-image yielding the displacement field, $u(\vec{r})$, with a spatial resolution of 20 nm. The stress field, $T(\vec{r'})$, was calculated:

$$u_i(\vec{r}) = \int \sum_j G_{ij}\left(\vec{r} - \vec{r'}\right) T_j\left(\vec{r'}\right) d\vec{r'}$$

where i and j denote spatial dimensions and G is the Green's tensor (which describes the response of the material to a punctual force)

Calculations were performed using Fast Fourier transform traction cytometry assuming that the substrate was of infinite thickness, and was homogenous, linearly elastic and isotropic. Only forces tangential to the imaging plane are considered reducing the problem to 2D.

Orientation analysis was performed by calculating the first order moment of the force distribution, or force dipole, which describes the contraction/dilation force as well as the torques applied by the cell:

$$M = \begin{bmatrix} \int xT_x & \int xT_y \\ \int yT_x & \int yT_y \end{bmatrix}$$

As the net torque is expected to be zero, the symmetrical matrix can be used to find the principle contractile axes: two contractile dipoles along two principal directions, corresponding to the two eigenvectors of the first order moment. The ratio, $\frac{(\lambda_1 - \lambda_2)}{(\lambda_1 + \lambda_2)}$, where λ_1 and λ_2 are the two eigenvalues of the first order moment tensor, has a value between 0 and 1. It indicates the degree of polarization of the force pattern.

QUANTIFICATION AND STATISTICAL ANALYSIS

Statistical analysis was performed using GraphPad Prism 9 software. All statistical tests and number of independent experiments are mentioned in the figure legends. Statistical significance is indicated as follows: *: p-value < 0.05; **: p-value < 0.01; ***: p-value < 0.001; ****: p-value < 0.0001.